



The Uncertainty of Local Background Magnetic Field Orientation in Anisotropic Plasma Turbulence

F. Gerick, J. Saur, and M. von Papen

Institute of Geophysics and Meteorology, University of Cologne, Cologne, Germany; felix.gerick@uni-koeln.de

Received 2017 May 1; revised 2017 May 24; accepted 2017 May 26; published 2017 June 26

Abstract

In order to resolve and characterize anisotropy in turbulent plasma flows, a proper estimation of the background magnetic field is crucially important. Various approaches to calculating the background magnetic field, ranging from local to globally averaged fields, are commonly used in the analysis of turbulent data. We investigate how the uncertainty in the orientation of a scale-dependent background magnetic field influences the ability to resolve anisotropy. Therefore, we introduce a quantitative measure, the angle uncertainty, that characterizes the uncertainty of the orientation of the background magnetic field that turbulent structures are exposed to. The angle uncertainty can be used as a condition to estimate the ability to resolve anisotropy with certain accuracy. We apply our description to resolve the spectral anisotropy in fast solar wind data. We show that, if the angle uncertainty grows too large, the power of the turbulent fluctuations is attributed to false local magnetic field angles, which may lead to an incorrect estimation of the spectral indices. In our results, an apparent robustness of the spectral anisotropy to false local magnetic field angles is observed, which can be explained by a stronger increase of power for lower frequencies when the scale of the local magnetic field is increased. The frequency-dependent angle uncertainty is a measure that can be applied to any turbulent system.

Key words: magnetohydrodynamics (MHD) – solar wind – turbulence

1. Introduction

Turbulent flows in magnetized plasmas are anisotropic due to the presence of a magnetic field (see, e.g., reviews by Horbury et al. 2012 and Oughton et al. 2015). In contrast to the velocity field, no Galileo transformation exists for the magnetic field such that for a certain eddy (or turbulent structure), the magnetic field associated with larger eddies vanishes. Therefore, the magnetic field of all larger scales directly influences the smaller scales of turbulence.

Deciphering the anisotropic structure of plasma turbulence is a major challenge, and several models are debated in the literature (e.g., Matthaeus et al. 1990; Goldreich & Sridhar 1995; Bieber et al. 1996; Saur & Bieber 1999; Galtier et al. 2005; Boldyrev 2006; Galtier 2006; Beresnyak & Lazarian 2008; Howes et al. 2008, 2011; Boldyrev & Perez 2012; Narita 2015). For understanding the anisotropy of turbulence in magnetized plasmas, the spatial and temporal extents of the magnetic field controlling the orientation and the decay of the turbulent eddies of specific scales remain unclear but are of crucial importance.

Two approaches are commonly used to characterize the controlling scale of the magnetic field, referred to as the global and local frames (Maron & Goldreich 2001; Horbury et al. 2008; Beresnyak & Lazarian 2009; Cho & Lazarian 2009; Tessein et al. 2009; Chen et al. 2011; Matthaeus et al. 2012). In the global frame, the magnetic field $\mathbf{B}(t)$ is averaged over scales much larger than the correlation length of the turbulent fluctuations to obtain the global mean field \mathbf{B}_0 . In the local frame, by contrast, it is assumed that a magnetic field at scales on the same order as those given by the individual turbulent structure or eddy controls the anisotropy of the turbulence (Cho & Vishniac 2000; Maron & Goldreich 2001; Cho et al. 2002; Cho & Lazarian 2004).

These considerations on the controlling scales are relevant for magnetized plasmas whether observed in space or generated

in numerical simulations. They pose important questions if the turbulent flow contains fluctuations $\delta\mathbf{b} = \mathbf{B} - \mathbf{B}_0$ with a root mean square (rms) similar to or larger than the mean magnetic field obtained by averaging over global scales. In the case of $\mathbf{B}_0 \gg \delta\mathbf{b}$, the problem simplifies, because the local background field is approximately equal to the global mean field.

The solar wind is a medium in which the large-scale background magnetic field \mathbf{B}_0 , averaged over hours, days, or years, is often on the same order as the rms of the magnetic field fluctuations $\delta\mathbf{b}$. Solar wind studies using a global magnetic field frame only detected anisotropy in the power of the fluctuations, not in the spectral index (Tessein et al. 2009). By contrast, several studies using a local and scale-dependent magnetic field for the analysis have revealed anisotropy in both power and spectral index κ in the inertial range spectrum of solar wind data (Alexandrova et al. 2008; Horbury et al. 2008; Podesta 2009; Chen et al. 2010; Luo & Wu 2010; Wicks et al. 2010, 2011; Podesta 2013). Horbury et al. (2008), for the first time, analyzed the spectral index κ with respect to a background magnetic field using such a local frame. The observed spectrum showed a spectral index of -2 parallel compared to $-5/3$ perpendicular to the local magnetic field (see lower panel of Figure 2 in Horbury et al. 2008), which is in agreement with the predicted scalings of the critical-balance theory (Goldreich & Sridhar 1995). Besides the spectral index, other anisotropic properties have been successfully analyzed using a local and scale-dependent magnetic field (e.g., Salem et al. 2012; He et al. 2013; Bruno & Telloni 2015).

Here, we introduce a geometrical condition for the scales of the magnetic field that is necessary to observationally resolve anisotropy within measured or simulated data. This condition is given by the average uncertainty in the orientation of the local background magnetic field at a certain scale. This uncertainty in the orientation is measured by the angle of the local background magnetic field with respect to the orientation of the observed

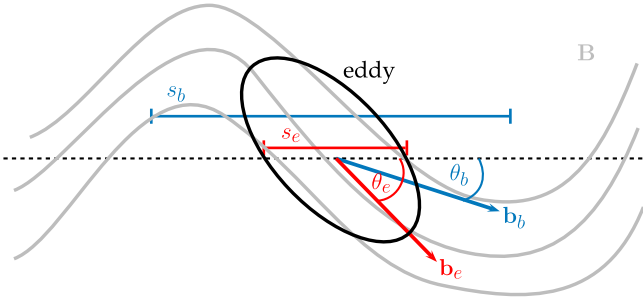


Figure 1. Schematic representation of the orientation of an eddy with respect to the orientation of two different background fields averaged at the scale of the eddy s_e and at some larger scale s_b .

fluctuations. This is referred to as ‘‘angle uncertainty’’ in the remainder of this work. To quantify the angle uncertainty in spacecraft measurements, we use the field-to-flow angle θ , which is defined as the angle between the magnetic field \mathbf{B} and the unperturbed flow direction of the solar wind \mathbf{v}_{SW} . In other systems, the orientation of the field may be conveniently defined in a different way.

The orientation of an elongated eddy within a magnetic vector field \mathbf{B} is shown schematically in Figure 1. Measuring along the dashed line, the magnetic field averaged over a scale s_e , which characterizes the size of an eddy (detailed definition in the following section), is associated with the angle θ_e . If the associated background magnetic field is defined over a larger scale s_b , the field-to-flow angle is θ_b . In this case, the fluctuations observed at the eddy scale are associated with a different field-to-flow angle. We hypothesize that, if the angle discrepancy between the scale at which the magnetic field is averaged and the eddy scale grows beyond a certain threshold, the angle of the local magnetic field is no longer well estimated. Therefore, the anisotropic properties of turbulent eddies might not be resolved under the assumption that the orientation of the eddies adjusts locally to the magnetic field.

In the following, we define the necessary scales, give a mathematical definition of the background magnetic field for different levels of localizations, and formally introduce the angle uncertainty as a measure of the orientation of an eddy within such averaged magnetic fields. Subsequently, we apply it to 91 days of magnetic field measurements within the fast solar wind (Wicks et al. 2010) and explore its suitability as a necessary condition for resolving observed or expected solar wind spectral anisotropy.

2. Analysis of Spectral Anisotropy

2.1. Relevant Scales and Wavelet Method

To analyze the spectral properties of turbulent fluctuations, we use a method based on the wavelet transformation. We denote $B_i(t)$, where $i = R, T, N$, as the magnetic field components measured as a function of time t in the RTN coordinate system.¹

¹ The unit vector \mathbf{e}_R points radially away from the Sun, $\mathbf{e}_T = \mathbf{e}_\Omega \times \mathbf{e}_R$ is perpendicular to \mathbf{e}_R and the Sun’s rotational axis \mathbf{e}_Ω , and $\mathbf{e}_N = \mathbf{e}_R \times \mathbf{e}_T$ completes the right-handed system.

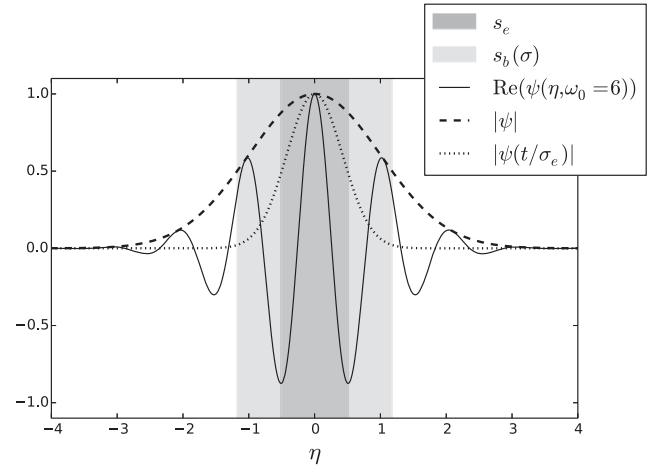


Figure 2. Real part of the normalized Morlet wavelet in time domain with the amplitude envelope (dashed), the Gaussian with standard deviation σ_e (dotted), and the two characteristic timescales s_e (dark gray) and $s_b(\sigma)$ (light gray).

The wavelet transformation of the components $B_i(t)$ is calculated as

$$W_i(t, \sigma) = \frac{1}{\sqrt{\sigma}} \int B_i(t') \psi\left(\frac{t' - t}{\sigma}\right) dt', \quad (1)$$

where $\psi(\eta)$ is the mother wavelet and σ is the wavelet scale. The absolute squared values of the complex wavelet coefficients, $|W_i(t, \sigma)|^2$, give the energy density at a time t and wavelet scale σ . In the case of the Morlet wavelet,

$$\psi(\eta) = \pi^{-1/4} e^{-i\omega_0\eta} e^{-\eta^2/2}, \quad (2)$$

the wavelet scale is the standard deviation of the Gaussian amplitude envelope of the wavelet, displayed as a dashed line in Figure 2 (Torrence & Compo 1998). The width of the wavelet can thus be defined by the full width at half maximum of the Gaussian window $2\sqrt{2\ln(2)}\sigma$ (light gray area in Figure 2). The wavelet packet given by Equation (2) can be associated with two scales. One scale, s_e , is associated with the period (frequency) of the fluctuations of the turbulent eddy that is to be analyzed. The other scale, s_b , is associated with the full width at half maximum of the wavelet, which constrains the temporal resolution and is used in the following section for the definition of the local background magnetic field.

The translation from wavelet scale to frequency,

$$f_e = (\omega_0 + \sqrt{2 + \omega_0^2}) / (4\pi\sigma), \quad (3)$$

depends on the number of oscillations ω_0 within the wavelet (Meyers et al. 1993). Here, we use $\omega_0 = 6$ so that $f_e = (1.033\sigma)^{-1}$. We define the scale s_e of the eddy under consideration as one period of the frequency $1/f_e$ (Figure 2, dark gray area) independent of the choice of ω_0 . The energy density of the wavelet coefficients can be associated with the eddy frequency f_e , which is consistent with the classical Fourier analysis commonly used in turbulence analysis.

To associate a local background magnetic field to each wavelet coefficient, one can use a Gaussian with a standard deviation $\sigma_b = \sigma$. This is a reasonable choice, as it describes the scale over which the energy density in the wavelet is calculated (Horbury et al. 2008). In the remainder of this work, we also investigate background magnetic fields averaged over

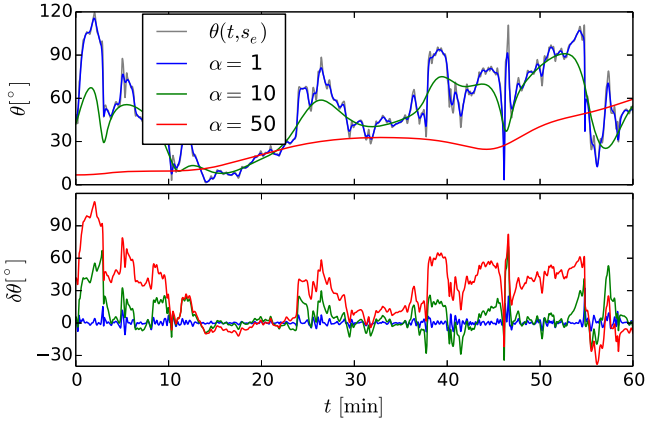


Figure 3. Figure shows $\theta(t, s_b)$ (top) and $\delta\theta(t, s_b, s_e)$ (bottom) at frequency $f_e = 0.1$ Hz for different averaging scales s_b of the local background magnetic field in 1 hr of *Ulysses* solar wind data (1995, DOY 100, 01:00:55–02:00:55).

larger scales using Gaussian windows with a standard deviation $\sigma_b > \sigma$. We therefore use a local, scale-dependent background magnetic field b_i for each component i , given by

$$b_i(t, s_b) = \int B_i(t') \exp\left(\frac{-(t' - t)^2}{2\sigma_b^2}\right) dt', \quad (4)$$

the convolution of the magnetic field with a Gaussian (Horbury et al. 2008; Podesta 2009). We introduce a dimensionless factor α , so that $\sigma_b = \alpha\sigma$, to quantify the increase of the averaging width. In the case of $\alpha = 1$, the averaging width corresponds to the envelope of the wavelet. The total averaging scale is $s_b(\sigma_b) = 2\sqrt{2\ln(2)}\sigma_b$. Standard deviations smaller than $\sigma_b = \sigma$ should not be used to average the magnetic field, since the energy density of the associated wavelet coefficients would correspond to wavelets larger than the averaged magnetic field.

The ratio of the smallest possible averaging scale and the eddy scale,

$$\frac{s_b(\sigma)}{s_e} = \frac{2\sqrt{2\ln(2)}(\omega_0 + \sqrt{2 + \omega_0^2})}{4\pi}, \quad (5)$$

depends only on the choice of ω_0 . This ratio is always larger than one and increases with larger ω_0 . The most local choice would be $\omega_0 = 6$, as $\omega_0 < 6$ fails the admissibility condition of wavelets (Farge 1992). That is why there is a minimum difference between s_e and s_b for wavelet-based analysis. For $\omega_0 = 6$, the minimum averaging scale $s_b(\sigma)$ is 2.28 times larger than s_e .

2.2. Field-to-Flow Angles and Uncertainty

To compute a field-to-flow angle,

$$\theta(t, s_b) = \cos^{-1}\left(\frac{\mathbf{b}(t, s_b) \cdot \mathbf{v}_{\text{sw}}}{|\mathbf{b}(t, s_b)| |\mathbf{v}_{\text{sw}}|}\right), \quad (6)$$

one can use the local background magnetic field vector $\mathbf{b}(t, s_b)$ obtained from Equation (4). This gives the angle between the (local) background magnetic field and the average solar wind velocity \mathbf{v}_{sw} . The second angle, which describes the orientation of the local background magnetic field, is the azimuth angle, but studies have shown that spectral anisotropy is approximately azimuthally symmetric around the local background

magnetic field (Horbury et al. 2008; Podesta 2009). We therefore only consider θ to characterize the variability of the orientation of the magnetic field.

The global power spectral density (PSD) at a distinct field-to-flow angle and with a temporal resolution Δt can be obtained from the wavelet coefficients by

$$P(f_e; \theta) = \sum_{i=R,T,N} P_i(f_e; \theta), \quad (7)$$

where

$$P_i(f_e; \theta) = \frac{2\Delta t}{N} \sum_{j=1}^N |W_i(t_j, \sigma; \theta)|^2 \quad (8)$$

is computed from N wavelet coefficients $W_i(t_j, \sigma; \theta)$ associated with the angle $\theta(t_j, s_b)$. In our analysis, we calculate the average $P(f_e; \theta)$ within bins of $\theta = 0^\circ\text{--}10^\circ, 10^\circ\text{--}20^\circ, \dots, 80^\circ\text{--}90^\circ$.

We average the magnetic field time series according to Equation (4) and calculate scale-dependent angles that characterize the orientation of an associated local background magnetic field according to Equation (6). We now define the angle uncertainty,

$$\delta\theta(t, s_b, s_e) = \theta(t, s_e) - \theta(t, s_b). \quad (9)$$

This angle quantifies the difference in magnetic field orientation between the eddy of scale s_e and the (larger) scale s_b over which the local magnetic field is defined.

We hypothesize that this newly introduced quantity is an indication of how local an averaged magnetic field is. The rms of the angle uncertainty $\delta\theta$ can be used to describe the average uncertainty of the orientation of eddies of size s_e when their orientation is measured with respect to a larger local background magnetic field. A minimum uncertainty arises from the difference between the background magnetic field averaged at scale s_b and the magnetic field averaged with a Gaussian of standard deviation $\sigma_e = (2\sqrt{2\ln(2)})^{-1}s_e$, which corresponds to the scale of the eddy fluctuations s_e (shown in Figure 2 as a dotted line). The minimum uncertainty is an inevitable consequence of wavelet analysis, as the energy density at the eddy scale s_e is averaged over the width of the wavelet $s_b(\sigma)$. The frequency uncertainty of the wavelet transform as an additional factor in the angle uncertainty is neglected, as it is found to be insignificant compared to the difference between s_e and $s_b(\sigma)$.

In the following, we use the rms of $\delta\theta$ to analyze the influence of the angle uncertainty on plasma turbulence properties, i.e., spectral anisotropy at magnetohydrodynamic (MHD) scales discussed here.

3. Solar Wind Observations

3.1. Angle Uncertainty and Spectral Anisotropy

We now investigate the scale dependence of the rms of the angle uncertainty $\delta\theta$ and how it is related to the ability to resolve the spectral anisotropy. We use 91 days of fast solar wind data with a resolution of 1 s from the *Ulysses* spacecraft from 1995, days 100–190, during a polar orbit at around 1.4–1.9 au (Balogh et al. 1992; McComas et al. 2000; Wicks et al. 2010). Similarly, and for comparison with Horbury et al. (2008), the mean flow velocity of the solar wind is assumed to be in the radial direction. For the time intervals used in this

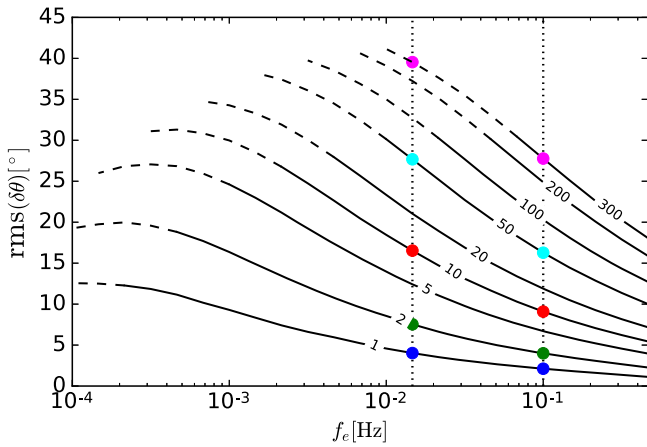


Figure 4. Rms of $\delta\theta$ as a function of eddy frequency f_e at different factors $\alpha = 1, \dots, 300$ (indicated by line numbers) of the minimum averaging width for characterizing a local background magnetic field. The areas averaged at scales larger than the outer scales $L \sim 1.5 \times 10^6$ km (Wicks et al. 2010) and $v_{sw} \approx 760$ km s $^{-1}$ are indicated by dashed lines. The dotted vertical lines represent the boundary frequencies used for spectral index fitting, and the colored circles aid comparison with Figures 6 and 7.

study, the deviation between the radial direction and the measured solar wind flow is, on average, 2° and can be neglected. We calculate the angle-resolved PSD according to Equation (8) and the angle uncertainty according to Equation (9) for several different scales on which the average magnetic field is calculated ($\alpha = 1$ –300).

Figure 3 shows an example of $\theta(t, s_b)$ (top) and $\delta\theta(t, s_b, s_e)$ (bottom) at eddy frequency $f_e = 0.1$ Hz in 1 hr of solar wind data. Three different averaging scales $s_b(\alpha\sigma)$ are displayed. For $\alpha = 1$, $\theta(t, s_b)$ is almost indistinguishable from $\theta(t, s_e)$, and $\delta\theta$ is small (rms = 3°). The larger the averaging scale s_b represented by the factor α , the larger the values of $\delta\theta$. At a factor $\alpha = 50$, the angle θ as a function of time becomes fairly smooth compared to the highly fluctuating $\theta(t, s_e)$. The resultant $\delta\theta$ for $\alpha = 50$ varies strongly and shows values up to 90° .

The rms of the angle uncertainty $\delta\theta$ for the complete data set is shown in Figure 4 as a function of the eddy frequency f_e . We see that the rms of the angle uncertainty increases with the width of the background magnetic field expressed through the factor α . This increase is expected from the sample values shown in Figure 3. The rms($\delta\theta$) also increases as the frequency f_e decreases, which may be explained by the power-law increase of power toward lower frequencies in the turbulent cascade. The dotted lines mark the frequency range 15 mHz $< f_e < 100$ mHz, considered to be the inertial range and used later to estimate the spectral index (Horbury et al. 2008). In this range, rms($\delta\theta$) reaches values between 7° and 12° for $\alpha = 5$. For small factors of α , around 2–3, the rms of the angle uncertainty is below 10° . At very large factors, $\alpha \geq 50$, the rms is over 25° , and the averaging scales reach the length of the outer scale (dashed lines in Figure 4), estimated to be $L \sim 1.5 \times 10^6$ km by Wicks et al. (2010). As the power depending on the angle is sorted into 10° bins, one might expect that the spectral anisotropy vanishes at factors $\alpha \geq 5$, because the rms of the angle uncertainty grows larger than the angle bin. We will analyze this aspect in detail later in this paper.

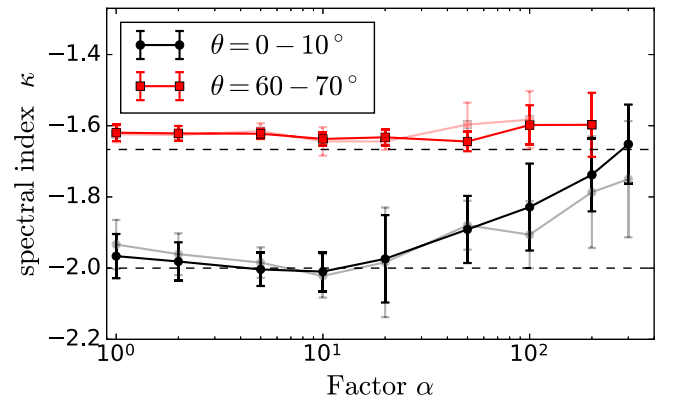


Figure 5. Spectral index κ at $\theta = 0^\circ$ – 10° and $\theta = 60^\circ$ – 70° as a function of increased averaging width by factor α . Error bars show the 95% confidence interval of the least-squares fit to $P(f_e; \theta)$. Light red and gray lines indicate the spectral indices from the 31 day data (DOY 100–130) from *Ulysses* (Horbury et al. 2008). We show angles between $\theta = 60^\circ$ and 70° , as a meaningful average for $\theta = 80^\circ$ – 90° was not available for large averaging widths.

For the spectral index analysis, we compute the power spectra $P(f_e; \theta)$ and determine the spectral indices in the range of 15 mHz $< f < 100$ mHz for each $\theta(t, s_b(\alpha\sigma))$ bin. The spectral indices at low (0° – 10°) and high (60° – 70°) angles for each factor α are shown in Figure 5. Error bars denote the 95% confidence interval of the least-squares fit in log-space. We show the spectral index at 60° – 70° because there are not enough coefficients with angles 80° – 90° to compute a meaningful average. However, the spectral index is approximately constant for angles $\theta > 50^\circ$ (Horbury et al. 2008; von Pappen & Saur 2015), and, therefore, the angle bin 60° – 70° represents the perpendicular case. For $\alpha = 1$, the analysis is similar to those of Horbury et al. (2008) and Podesta (2009), and the spectral indices are in agreement with the anisotropic scaling predicted by the critical-balance theory (Goldreich & Sridhar 1995). It shows a spectrum f^{-2} parallel and $f^{-5/3}$ perpendicular to the local background magnetic field (see Figure 5, $\alpha = 1$). We note that the spectral anisotropy is maximal not for $\alpha = 1$ but for $\alpha = 10$. However, the difference between the parallel spectral indices corresponding to these factors is small and within the error bars. For factors $\alpha > 10$, the anisotropy slowly decreases. This is also observed in the shorter 31 day data set used by Horbury et al. (2008), which spans DOY 100–130 of 1995 and is shown with light red and gray lines in Figure 5. The spectral index of the perpendicular cascade is not affected by the scale of the background field. The reason is that, for $\alpha = 1$, the spectral index as a function of the field-to-flow angle θ near 0° changes very rapidly with growing θ , while it is almost constant at $-5/3$ for field-to-flow angles in the range 30° – 90° (see Figure 2 in Horbury et al. 2008). Additionally, the power at smaller angles is sufficiently smaller compared to the power at larger angles, which thus dominate the spectral contributions (again, see Figure 2 in Horbury et al. 2008). The factors $\alpha > 100$ correspond to a local field so large—namely, averaged over $s_b = 4.5$ hr at 15 mHz—that it can be regarded as a global background field. Accordingly, the spectral anisotropy is not resolved for a global field. This is, to our knowledge, the first time that a gradual change of the spectral anisotropy from the local to the global field has been shown.

The robustness of the spectral index for factors $5 < \alpha < 20$ is unexpected. The previously introduced rms of the angle

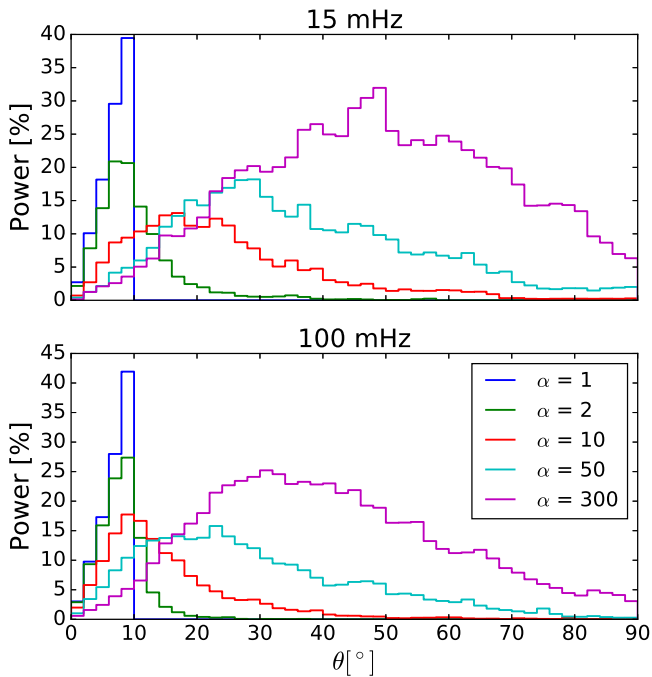


Figure 6. Origin θ of the power for the wavelet coefficients originally within the 0° – 10° bin for $\alpha = 1$ at 15 mHz (top) and 100 mHz (bottom). Percentages of power are with respect to the total power in the 0° – 10° bin at $\alpha = 1$. For larger factors $\alpha > 1$, the power additionally comes from larger field-to-flow angles. It can be seen that false coefficients first contribute to low frequencies. For $\alpha = 10$, e.g., the maximum power comes from 20° at 15 mHz but from 10° at 100 mHz.

uncertainty suggests that anisotropy might not be resolved for factors $\alpha \geq 5$, since a strong variability of the spectral index for $\theta < 30^\circ$ – 40° is observed and a resolution of 10° is necessary (see lower panel of Figure 2 in Horbury et al. 2008). To explain this discrepancy between the observed spectral anisotropy and the observed rms of the angle uncertainty, we now study how accurately the wavelet coefficients are associated with the angle bins under consideration.

3.2. Origin of Power in the Parallel Angle Bin

In Figure 4, we show that large scales of the local background field lead to large angle uncertainties. This can be interpreted in the sense that a large-scale local background magnetic field, i.e., a background magnetic field with factors $\alpha \geq 5$, is not an adequate representation of the orientation of the turbulent fluctuations. Mathematically, this means that wavelet coefficients $W(t, f_e, \theta)$ are not assigned to the correct angle.

We now investigate if and how many wavelet coefficients associated with larger angles $\theta(\alpha = 1) > 10^\circ$ at the most local scale are falsely assigned to the angle bin 0° – 10° when the local background field is large ($\alpha = 2$ – 300). In the following, we refer to wavelet coefficients originating from higher angles and being assigned to the 0° – 10° bin as “false” coefficients.

We compute the angular origin $\theta(\alpha = 1)$ of larger-scale ($\alpha > 1$) coefficients within the 0° – 10° bin for the upper (100 mHz) and lower (15 mHz) frequency boundary of the fit range. The result tells us how many false coefficients contribute to the power $\sum |W(\theta(\alpha))|^2$ within the $0^\circ \leq \theta(\alpha) < 10^\circ$ bin and is shown in Figure 6. To aid visualization of the redistribution of the angle bins for growing α , we choose a

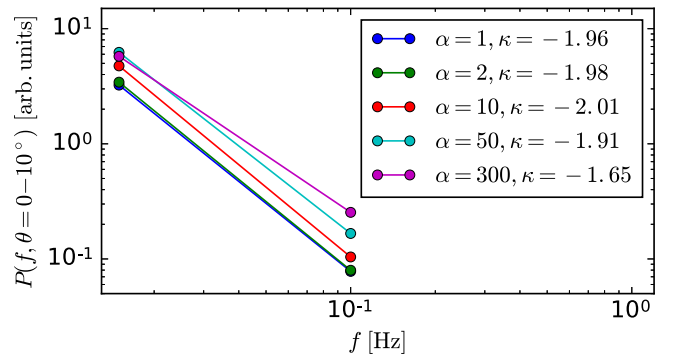


Figure 7. PSD and spectral index κ at $\theta = 0^\circ$ – 10° at the factors 1, 2, 10, 50, and 300 in blue, green, red, cyan, and magenta, respectively. Only 15 and 100 mHz frequencies are shown to aid comparison to Figure 6 and visualization of the slopes.

bin resolution of 2° . The histograms are normalized to the total power in the 0° – 10° bin at $\alpha = 1$. It can be seen that, if we use larger and larger averaging widths, the power spectra include more and more false coefficients with angles originally outside the 0° – 10° bin. For $\alpha = 10$, we observe that, for 15 mHz, the maximum of the coefficients actually stems from angles around 20° , and thus the power has large contributions from false coefficients. The corresponding rms of the angle uncertainties associated with this averaging width $\alpha = 10$ assumes values larger than 15° (shown in Figure 4).

To understand the influence of the origin of the power presented in Figure 6 on the slope of the power spectra, we compute the PSD for several averaging widths in Figure 7. For $\alpha = 2$, the contribution of power from larger angles is low, and, therefore, the spectral energy distribution $P(f; \theta = 0^\circ$ – $10^\circ)$ at $\alpha = 2$ is almost identical to $P(f; \theta = 0^\circ$ – $10^\circ)$ at $\alpha = 1$ (see Figure 7, green and blue lines). For $\alpha = 50$, most of the coefficients are falsely associated with contributions from angles of 20° and 30° for 15 and 100 mHz, respectively. This shows how large averaging widths smooth out local small-scale variations and may thus lead to a false angle association. However, as power from larger angles at increasing factors does not contribute equally to the 0° – 10° bin for 15 and 100 mHz, the slope appears to be similar. The power of larger angles associated with the $\theta = 0^\circ$ – 10° bin at $\alpha = 10, 50$ (Figure 6, red and cyan lines) for 15 mHz is much larger than that for 100 mHz. From this, it follows that the spectral index can still be as steep as -2 and even steeper than at $\alpha = 1$, but the total power clearly increases. Due to this unequal contribution of the power of larger angles at different frequencies, the spectral index can remain as steep as -2 to factors of $\alpha \approx 20$ – 50 even though power is added to the parallel spectrum. For an increased averaging width by a factor of $\alpha \geq 50$, the spectral index still shows anisotropy but is more shallow than -2 . For $\alpha \geq 200$, the parallel spectral index is $-5/3$, and no spectral anisotropy can be resolved (see Figure 5). Despite the fact that κ stays around -2 for α up to 50, the magnetic field averaged at factors $\alpha > 5$ should not be considered an appropriate local background magnetic field, as false coefficients contribute to the power.

4. Discussion and Conclusions

We have introduced the angle uncertainty between the orientations of the averaged magnetic field and the eddy fluctuations as a measure to describe the uncertainty of the

orientation of a (local) background magnetic field, and thus as a measure to resolve the anisotropy of turbulent properties. We studied the scale-dependent angle uncertainty and how it is related to the resolution of the spectral anisotropy in fast solar wind data.

The rms of the angle uncertainty $\text{rms}(\delta\theta)$ depends on the frequency/eddy size of the fluctuation. A finite rms implies the existence of a basic, frequency-dependent uncertainty to resolve anisotropy. We investigated previously observed anisotropy with a resolution of 10° (Horbury et al. 2008). Only if the rms of the angle uncertainty is lower than 10° can the correct association of magnetic field orientation to the wavelet coefficients be assured. Based on the results presented in Figure 4, such a correct association is obtained for averaging widths $\alpha \leq 4$, which corresponds to $s_b \leq 10s_e$. It is apparent that the definition of a local background magnetic field depends on the frequency range or eddy size under consideration and on the anisotropy to be resolved. Anisotropy that is sensitive to changes below 10° would require smaller averaging scales of the magnetic field to resolve such an anisotropy, in case the distribution of scale-dependent energy is similar to the case studies given here.

The solar wind observations presented in this work show that the observed spectral anisotropy is no longer adequately resolved for $\alpha \geq 50$ and vanishes for $\alpha \geq 200$, i.e., an averaging width more than 200 times larger than the eddy scale. Although the rms of the angle uncertainty at factors $\alpha \geq 5$ is larger than the width of the angle bin, the spectral index remains anisotropic. This unexpected apparent robustness of the spectral anisotropy with respect to the increased averaging width can be explained by a frequency-dependent gain of power from the wavelet coefficients of higher angles. Higher frequencies gain less power from wavelet coefficients associated with higher angles than lower frequencies (see Figure 6). The origin of the power, meaning the angles associated with the power when averaging with $\alpha = 1$, at different frequencies is in agreement with the frequency-dependent rms of the angle uncertainty. Even though the total power at small angles clearly increases for increasing factors α (see Figure 7), the slope of the PSD remains steep even for very large averaging widths. The apparent robustness to the increased averaging width should therefore not lead to an incorrect conclusion on the size of a local background magnetic field. The rms of the angle uncertainty predicts the error in the association of the wavelet coefficients, and, for $\alpha \geq 5$, the total power in the parallel spectrum clearly increases. Only the anisotropy in the spectral index appears to be intact due to the effect of the frequency-dependent power gain.

Within the studied data set, a magnetic field averaged at $\alpha \approx 5-50$ may be regarded as an intermediate background magnetic field, not local or global. For an intermediate background magnetic field, although scale-dependently averaged, the rms of the angle uncertainty $\text{rms}(\delta\theta)$ within the frequency range under consideration is larger than the accuracy needed (10°), and the wavelet coefficients may not be linked to the correct angle.

At even larger averaging scales, corresponding to $\alpha \geq 50$, the background magnetic field approaches the global mean magnetic field, for which the averaging is performed over the complete data interval (Oughton et al. 2015). Even if a local magnetic field is used that is on the order of the outer scale $L \sim 1.5 \times 10^6$ km (Wicks et al. 2010), it may be regarded as the global mean field. The rms of the angle uncertainty $\text{rms}(\delta\theta)$ within the analyzed

frequency range exceeds 25° for averages over scales larger than the outer scale (see Figure 4, dashed lines). In this case, a significant amount of power cannot be linked correctly to a field-to-flow angle bin.

For comparison between the local and global background magnetic fields, we also analyzed the data using a scale-independent background field (not shown). Here, the power of eddies at different scales is associated with the same background magnetic field. We were unable to observe spectra that scale with f^{-2} parallel to the background magnetic field using such a global frame. The rms of the angle uncertainty of such a scale-independent magnetic field also depends on the frequency under consideration. When averaging with a window width of 5 times the largest period (5×67 s) of the frequencies within which spectral indices are calculated, the rms of the angle uncertainty ranges from 7° at low frequencies to 10° at high frequencies (see Figure 4 at $\alpha \approx 2$ for 15 mHz and $\alpha \approx 13$ for 100 mHz). Eddies of lower frequency with periods closer to the averaging scale might be represented well enough by such a background magnetic field. However, as higher frequencies are analyzed with the same background magnetic field, the power of these eddies is associated with an angle resulting from larger-scale fluctuations. Consequently, more power from false coefficients contributes to the higher-frequency fluctuations, whereas very little (or none) contributes to the lower-frequency fluctuations. Following this, the effect that the spectral index can remain steep, observed for scale-dependent magnetic fields, does not hold for the global approach. Note that, in the limit of a very strong background magnetic field, where $|\mathbf{B}_0| \gg |\delta\mathbf{b}|$, the values of $\delta\theta$ decrease and may have a negligible frequency dependency, and the global approach will be applicable.

The angle uncertainty presented here provides an uncertainty measure of the orientation of turbulent structures/eddies as a function of the scale of the averaged magnetic field and of the associated frequency/period of the eddies under investigation. This method, however, does not constrain the scale of the wave numbers of the eddies in directions parallel and perpendicular to the associated background magnetic field. The reason is that, under the assumption of Taylor's hypothesis (Taylor 1938) and the spatial and temporal stationarity of the magnetic field, wave vectors of different magnitude and orientation contribute to the spectral energy density at one frequency f_e (e.g., Fredricks & Coroniti 1976; von Papen & Saur 2015).

The angle uncertainty is physically controlled by two effects: (a) the frequency/scale-dependent amplitudes of the turbulent fluctuations and (b) any nonturbulent contributions, such as the magnetic field convected out from the solar corona. These contributions generate the total field, which controls the orientation of the turbulent eddies. Thus, the contribution of the solar background field (Parker 1958) with respect to the amplitude of the fluctuations plays an important role in the angle uncertainty. For example, for magnetic field fluctuations $\delta\mathbf{b}$ much smaller than the amplitude of the global mean magnetic field \mathbf{B}_0 , the angle uncertainty would tend to small values, and anisotropy should be well resolved. The ability to resolve anisotropy as a function of scale is not universally equal but depends on the turbulent system, for example, on the values of the spectral slopes of the energy distribution. The angle uncertainty is a helpful measure that can be applied to various systems to evaluate the ability to resolve anisotropy to a certain degree.

References

- Alexandrova, O., Lacombe, C., & Mangeney, A. 2008, *AnG*, **26**, 3585
- Balogh, A., Beek, T., Forsyth, R., et al. 1992, *A&AS*, **92**, 221
- Beresnyak, A., & Lazarian, A. 2008, *ApJ*, **682**, 1070
- Beresnyak, A., & Lazarian, A. 2009, *ApJ*, **702**, 460
- Bieber, J. W., Wanner, W., & Matthaeus, W. H. 1996, *JGRA*, **101**, 2511
- Boldyrev, S. 2006, *PhRvL*, **96**, 115002
- Boldyrev, S., & Perez, J. C. 2012, *ApJL*, **758**, L44
- Bruno, R., & Telloni, D. 2015, *ApJL*, **811**, L17
- Chen, C. H. K., Mallet, A., Yousef, T. A., Schekochihin, A. A., & Horbury, T. S. 2011, *MNRAS*, **415**, 3219
- Chen, C. H. K., Wicks, R. T., Horbury, T. S., & Schekochihin, A. A. 2010, *ApJL*, **711**, L79
- Cho, J., & Lazarian, A. 2004, *ApJL*, **615**, L41
- Cho, J., & Lazarian, A. 2009, *ApJ*, **701**, 236
- Cho, J., Lazarian, A., & Vishniac, E. T. 2002, *ApJ*, **564**, 291
- Cho, J., & Vishniac, E. T. 2000, *ApJ*, **539**, 273
- Farge, M. 1992, *AnRFM*, **24**, 395
- Fredricks, R. W., & Coroniti, F. V. 1976, *JGR*, **81**, 5591
- Galtier, S. 2006, *JPIPh*, **72**, 721
- Galtier, S., Pouquet, A., & Mangeney, A. 2005, *PhPI*, **12**, 092310
- Goldreich, P., & Sridhar, S. 1995, *ApJ*, **438**, 763
- He, J., Tu, C., Marsch, E., Bourouaine, S., & Pei, Z. 2013, *ApJ*, **773**, 72
- Horbury, T. S., Forman, M., & Oughton, S. 2008, *PhRvL*, **101**, 175005
- Horbury, T. S., Wicks, R. T., & Chen, C. H. K. 2012, *SSRv*, **172**, 325
- Howes, G. G., Cowley, S. C., Dorland, W., et al. 2008, *JGRA*, **113**, A05103
- Howes, G. G., TenBarge, J. M., & Dorland, W. 2011, *PhPI*, **18**, 102305
- Luo, Q. Y., & Wu, D. J. 2010, *ApJL*, **714**, L138
- Maron, J., & Goldreich, P. 2001, *ApJ*, **554**, 1175
- Matthaeus, W. H., Goldstein, M. L., & Roberts, D. A. 1990, *JGRA*, **95**, 20673
- Matthaeus, W. H., Servidio, S., Dmitruk, P., et al. 2012, *ApJ*, **750**, 103
- McComas, D. J., Barraclough, B. L., Funsten, H. O., et al. 2000, *JGRA*, **105**, 10419
- Meyers, S. D., Kelly, B. G., & O'Brien, J. J. 1993, *MWRv*, **121**, 2858
- Narita, Y. 2015, *AnG*, **33**, 1413
- Oughton, S., Matthaeus, W. H., Wan, M., & Osman, K. T. 2015, *RSPTA*, **373**, 20140152
- Parker, E. N. 1958, *ApJ*, **128**, 664
- Podesta, J. J. 2009, *ApJ*, **698**, 986
- Podesta, J. J. 2013, *SoPh*, **286**, 529
- Salem, C. S., Howes, G. G., Sundkvist, D., et al. 2012, *ApJL*, **745**, L9
- Saur, J., & Bieber, J. W. 1999, *JGRA*, **104**, 9975
- Taylor, G. 1938, *RSPSA*, **164**, 476
- Tessein, J. A., Smith, C. W., MacBride, B. T., et al. 2009, *ApJ*, **692**, 684
- Torrence, C., & Compo, G. P. 1998, *BAMS*, **79**, 61
- von Papen, M., & Saur, J. 2015, *ApJ*, **806**, 116
- Wicks, R. T., Horbury, T. S., Chen, C. H. K., & Schekochihin, A. A. 2010, *MNRAS*, **407**, L31
- Wicks, R. T., Horbury, T. S., Chen, C. H. K., & Schekochihin, A. A. 2011, *PhRvL*, **106**, 045001